ISBN: 978-3-95450-231-8 ISSN: 2673-5490 doi: 10.18429/JACoW-IPAC2023-TUPL149

DARK CURRENT IN THE LCLS-II-HE SUPERCONDUCTING INJECTOR*

S. T. Littleton† [1], T. O. Raubenheimer[1], C. Adolphsen, C. Mayes, F. Ji
SLAC National Accelerator Laboratory, Menlo Park, CA, United States
[1]also at Stanford University, Stanford, CA, United States

Content from this work may be used under the terms of the CC BY 4.0 licence (© 2022). Any distribution of this work must maintain attribution to the author(s), title of the work, publisher, and DOI.

Abstract

In high-gradient accelerator structures, field emission produces dark current that behaves much differently than the main photobeam current. This dark current can damage accelerator components and increase the radiation dose in the surrounding area. Thus it is important to analyze its behavior when designing a new accelerator or subsystem, such as the superconducting low-emittance injector (LEI) currently under development for the LCLS-II high-energy upgrade (LCLS-II-HE). In principle, the emission of dark current is governed by the Fowler-Nordheim (FN) equation. In practice, variations in surface quality result in localized emission sites at locations that are not predictable a priori. Since the superconducting gun for the LEI does not exist yet, particles must be tracked from a dense array of initial positions and times on all likely emission surfaces and assigned weights according to the FN equation in the early design phases to inform the placement of collimators. We present the results of tracking studies using BMAD and Python to analyze dark current in the LEI.

BACKGROUND PRINCIPLES

In the presence of intense electric fields, electrons are emitted from conducting surfaces in a process known as Fowler-Nordheim (FN) field emission. The physical mechanism responsible for this process is quantum tunneling. An analysis of the Schrödinger equation in a simplified potential function, consisting of a potential well within the conductor and a constant slope (representing the applied electric field) outside the conductor gives the result [1, 2]

$$J_{FN} \propto (\beta_{FN} E_{\perp})^2 \exp\left[-\frac{a_1}{\beta_{FN} E_{\perp}}\right], \qquad (1)$$

where a_1 is a material parameter that depends on the work function and β_{FN} is a scaling factor that relates the macroscopic electric field $E_{\perp}$ to the microscopic electric field seen by the electrons at the surface. In practice, we cannot know the exact value of β_{FN} at a given point. However, we can use common values for a given material to inform our expectations of the distribution of emitters, and to analyze the effectiveness of various collimation schemes in the design stage. In the ongoing design work for the LEI, we use Eq. 1 as a weight function to produce expected distributions of dark current at various points throughout the system.

SIMULATION APPROACH

Since the locations of dark current emission sites are not known a priori, particles were tracked from a dense collection of cathode radii from 0 to 10 mm and phases from $-\pi/8$ to $+\pi/8$ relative to the temporal center of the photoelectron beam. These particles were assigned weights according to the FN field emission intensity, which depends on the electric field magnitude at the location and time of emission. Particles emitted at relative phases outside of this small window around the peak have much lower FN weights and are poorly matched to the subsequent buncher and accelerator cavities. Thus, the little current that is generated outside of this window is either lost without significant power deposition or easily collimated in the energy collimator in the dogleg. Tracking was performed with the BMAD-based [3] `dark_current_tracker` program, using a custom Python toolbox as a controller and post-processor for large sets of tracking simulations with various beamline settings.

For this study, the “complex" layout of the LEI was assumed, with a 30 MV/m gradient at the cathode. As shown in Fig. 1, the complex layout consists of the superconducting electron gun, a solenoid at the gun exit, a normal-conducting buncher, a second solenoid 1.7 m from the cathode, a superconducting buncher, and a cryomodule consisting of eight superconducting nine-cell TESLA cavities, followed by a set of quadrupoles to match the beam from the injector to downstream components. Beyond that, there are two configurations: an achromatic dogleg that joins the rest of the linac and a diagnostic beamline, with the first dipole of the dogleg serving to switch between the two configurations.

Since the greatest field enhancement occurs near the gap between the cathode plug and the cavity wall, it was necessary to track the particles through the region within 1 mm of the cathode using a high-resolution field map. Figure 2 shows a sample of particle tracks within this region, with the tracks colored according to their FN weights. Electrons with the largest weights are emitted from a 3 - 5 mm radius on the cathode plug and from a 6 - 8 mm radius on the cavity wall. The large initial radii of these particles result in large transverse orbits. These orbits are further enlarged by overfocusing in the first solenoid, due to the lack of significant space charge effects in the low-density dark current. Consequently, much of the dark current will be blocked by the circular collimator that is located 1.7 m from the cathode, near the second solenoid. Figure 3 shows the expected dark current fraction that would be blocked by the collimator versus the collimator radius, and Fig. 4 shows how the radius at the collimator maps to the emission radius. This map is not one-to-one due to time-dependent field at the emission sites.

* WORK SUPPORTED BY THE U.S. DEPARTMENT OF ENERGY UNDER CONTRACT NO. DE-AC02-76SF00515.
† seantl@slac.stanford.edu

ISBN: 978-3-95450-231-8 ISSN: 2673-5490 doi: 10.18429/JACoW-IPAC2023-TUPL149

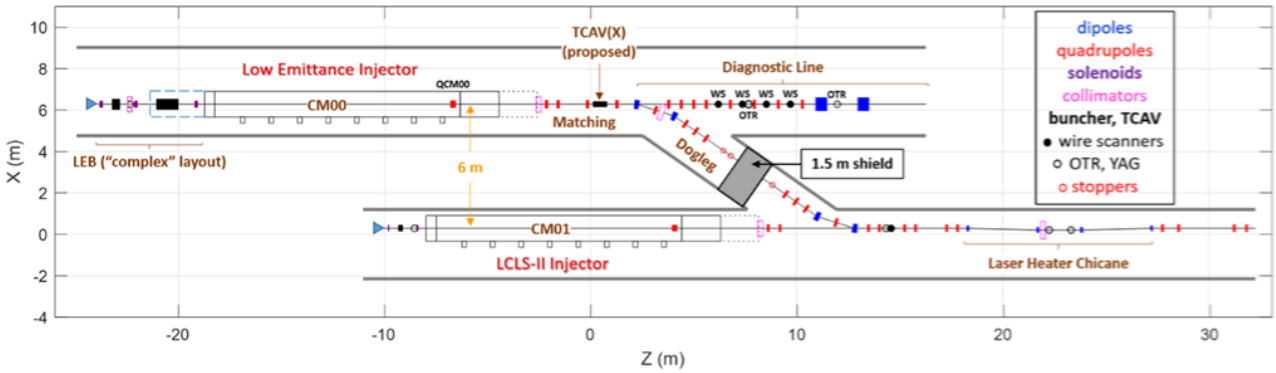

Figure 1: "Complex" layout of the LEI and the dogleg that brings the beam to the rest of the LCLS-II-HE linac.

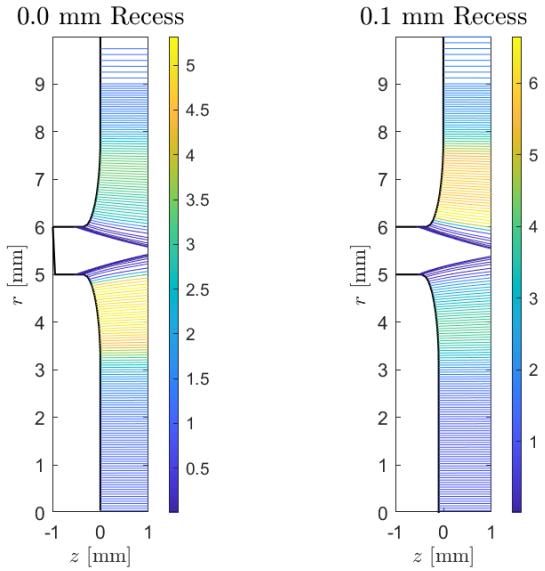

Figure 2: Particle tracks for the first millimeter off of the cathode plane, both for a cathode plug flush with the cavity wall and for a plug recessed by 0.1 mm. The tracks are colored by relative FN weights.

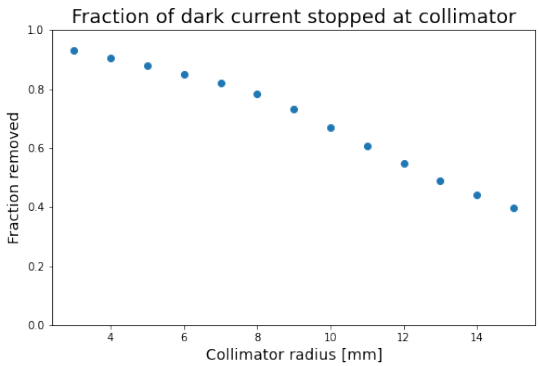

Figure 3: A 9 mm-radius collimator at $z = 1.7$ m intercepts about 73% of the dark current before it is accelerated in the cryomodules.

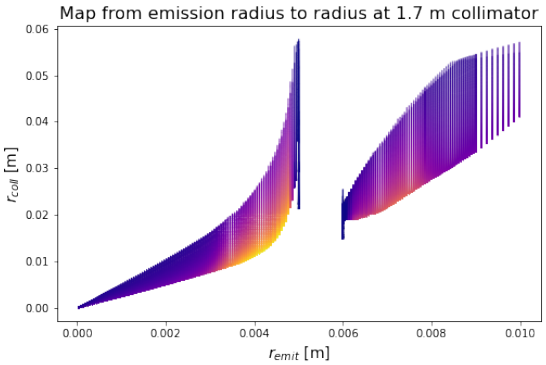

Figure 4: The transfer map from r_{emit} to r_{coll} is color-coded by Fowler-Nordheim weight at the time and location of emission, with brighter colors representing higher weights.

LOSS DISTRIBUTION

To understand the effectiveness of our collimation strategy, it is helpful to analyze the behavior of dark current emitted from different bands of radii. Figure 5 shows the dark current transmission along the beamline for several bands of emission radii with the energy collimator jaws set to ± 3 mm, which fully removes the low-energy peak. Importantly, no particles outside of the 5 mm radius of the cathode plug make it past a 9 mm radius collimator at $z = 1.7$ m. Once the gun cavity is installed, not much can be done to reduce the dark current from the niobium surface at a given gradient, whereas the cathode plug can be replaced if it is a major source of the dark current. Particles emitted from the cathode plug would be difficult to collimate due to their low betatron oscillation amplitudes, and would not be significantly attenuated until they reach the energy collimator in the dogleg. Fortunately, significant emission is only expected at radii greater than 3 mm, where early collimation at low energy is relatively easy due to the large amplitudes those particles reach at the location of the first collimator, just before the second solenoid. Almost all of the remaining dark current from likely emission locations in the gun is lost before reaching the main axis of the LCLS-II-HE accelerator.

Content from this work may be used under the terms of the CC BY 4.0 licence (© 2022). Any distribution of this work must maintain attribution to the author(s), title of the work, publisher, and DOI.

ISBN: 978-3-95450-231-8 ISSN: 2673-5490 doi: 10.18429/JACoW-IPAC2023-TUPL149

© Content from this work may be used under the terms of the CC BY 4.0 licence (© 2022). Any distribution of this work must maintain attribution to the author(s), title of the work, publisher, and DOI.

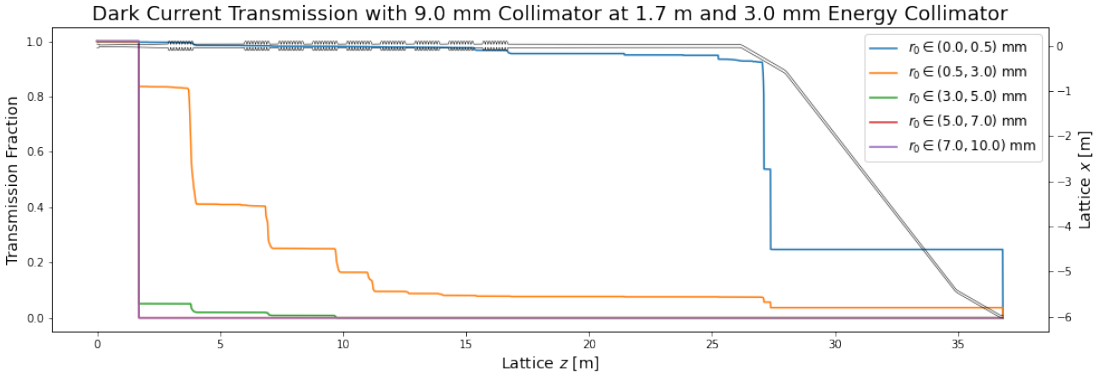

Figure 5: Transmitted dark current as a function of z, normalized to the total number emitted in each radial band.

ENERGY DISTRIBUTION

Figure 6 shows the energy distribution at the location of the first collimator, before entering the superconducting buncher. This distribution resembles the distribution observed when the dark current from the APEX gun was measured [4]. Although the geometry and materials in the superconducting gun differ significantly from the APEX gun, the longitudinal phase space should be qualitatively similar. A notable feature of the dark current distribution is a low-energy peak in the energy distribution, shown in Fig. 7. This peak can be removed by a judicious choice of the horizontal jaw setting of the energy collimator near the beginning of the dogleg, where the dispersion is about 20 cm.

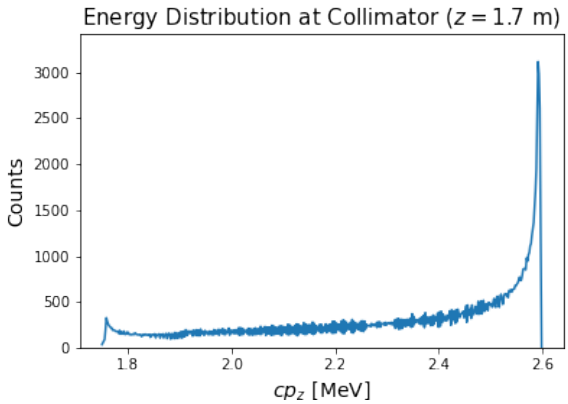

Figure 6: Energy distribution at the first collimator, near the second solenoid.

CONCLUSION

Although we cannot know where the dark current will originate from until the LEI is built and tested, we can use the Fowler-Nordheim equation to make informed choices regarding the placement, sizes, and settings of the collimators. Due to the large orbits of the dark current from likely emission sites, and its bimodal energy spectrum, we expect to be able to intercept the dark current before it is accelerated to higher energies in the linac.

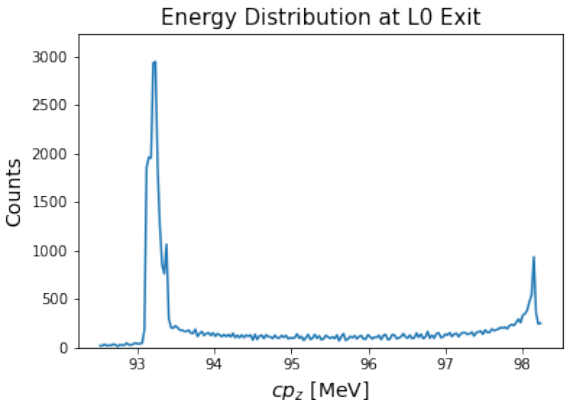

Figure 7: Energy distribution at the exit of the L0 cryomodule.

ACKNOWLEDGMENTS

This work is supported by the U.S. Department of Energy under Contract No. DE-AC02-76SF00515.

REFERENCES

[1] R. H. Fowler and L. Nordheim, "The effect of the image force on the emission and reflexion of electrons by metals," *Proc. R. Soc. Lond.*, vol. 119, pp. 173–181, 781 1928. DOI: 10.1098/rspa.1928.0091.

[2] L. W. Nordheim, "The effect of the image force on the emission and reflexion of electrons by metals," *Proc. R. Soc. Lond. A*, vol. 121, pp. 626–639, 788 1928. DOI: 10.1098/rspa.1928.0222.

[3] D. Sagan, "Bmad: A relativistic charged particle simulation library," *Nucl. Instrum. Meth.*, vol. A558, no. 1, pp. 356–359, 2006, Proceedings of the 8th International Computational Accelerator Physics Conference, ISSN: 0168-9002. DOI: https://doi.org/10.1016/j.nima.2005.11.001.

[4] R. Huang, D. Filippetto, C. F. Papadopoulos, H. Qian, F. Sannibale, and M. Zolotorev, "Dark current studies on a normal-conducting high-brightness very-high-frequency electron gun operating in continuous wave mode," *Phys. Rev. ST Accel. Beams*, vol. 18, p. 013 401, 1 2015. DOI: 10.1103/PhysRevSTAB.18.013401. https://link.aps.org/doi/10.1103/PhysRevSTAB.18.013401